Strongly perturbed Stark states and electron correlation in Ba

F. Robicheaux,[1,2] C. Wesdorp,[2] and L. D. Noordam[2]
[1]*Department of Physics, Auburn University, Auburn, Alabama 36849*
[2]*FOM Institute for Atomic and Molecular Physics, Kruislaan 407, 1098 SJ Amsterdam, The Netherlands*
(Received 17 November 1998)

We present the results of experimental and theoretical investigations into the photoionization spectra of Ba Stark states at energies resonant with the $5d7d\,^1D_2$ perturber level starting from the $5d6p\,^3D_1^o$ state. The electric field is strong enough to allow the electrons to classically escape the atom, thus transforming the perturber state into a resonance. Much of the dynamics of this remarkably complex system may be understood qualitatively. In particular, we stress the role played by electron escape time in qualitatively changing the correlation by reducing the singlet-triplet mixing and triplet excitation. A theoretical formulation of multichannel systems in static electric fields is developed which allows us to efficiently obtain both total and partial cross sections; this formulation can be used to describe the Rydberg states of atoms and molecules in static electric fields. [S1050-2947(99)11308-8]

PACS number(s): 32.60.+i, 32.80.Dz, 32.80.Fb

I. INTRODUCTION

One of the main goals of atomic physics involves the qualitative and quantitative understanding of the dynamics of valence electrons. An important variant of these studies concentrates on the dynamics of atoms in static fields. Static fields generate a more complicated set of energy levels and eigenstates since the total angular momentum is no longer conserved. But surprisingly, the resulting richness and complexity can often be interpreted with qualitative ideas that do not involve elaborate calculations. Atomic dynamics in static electric fields is also important in that the electric field can strongly affect the rate that ions capture electrons into bound states through photorecombination.

In this paper, we present recent experimental and theoretical results for Ba in a static electric field at energies near the $5d7d\,^1D_2$ perturber level [1,2]; this state perturbs the $6snd\,^1D_2$ and $^3D_2$ series from $n=25$–28. Although the electric field strongly mixes states of different angular momentum and parity, we find that the $5d7d\,^1D_2$ perturber does introduce complexities not found in atomic systems away from short range resonances. Even in zero field, the number (and complexity) of all the J^π states in this energy region is quite high [3,4] compared to what is usually included in photoionization studies because usually only a small subset of states are considered because of selection rules; there are 20 channels with nonzero K-matrix elements attached to the $6s$ threshold and 100 channels attached to the $5d$ threshold. We obtain excellent agreement between theory and experiment, which indicates that all of the important mechanisms for describing complex Stark resonances are understood. We obtain a qualitative level of understanding of this system, which is important for generalizing these techniques to other atoms and to molecules. In particular, this system clearly shows that channel mixing depends on the short-range channel interactions *and* the asymptotic (large r) dynamics in the channels. This aspect of our qualitative understanding clarifies our interpretation of the zero-field dynamics of Ba in which it is often forgotten that the mixing between states is also determined by the large r boundary conditions on the wave function.

The spectrum of an H atom in a static electric field (assumed to be in the z direction) is relatively simple because the wave function is separable in parabolic coordinates; $r+z$, $r-z$, and φ. The spectrum of an alkali-metal atom in an electric field is much more complicated because this separation is no longer possible. Spherical coordinates are appropriate near the nucleus, while parabolic coordinates are more appropriate outside the region occupied by the core electrons. The alkali Stark states result from coupled multichannel dynamics [5]. The channels are defined in parabolic coordinates in order to correctly describe the large r behavior of the wave function, and the coupling arises when the electron enters the region of the core electrons and scatters from one parabolic channel to another. While the scattering can change the parabolic quantum numbers, it cannot change m, the z component of the angular momentum.

Recent investigations [6–13] of non-alkali-metal atoms raise the level of complexity and extend accurate Stark calculations to several types of atoms in the periodic table. The additional complexity arises because the Rydberg electron can scatter from the core electrons and change its energy, angular momentum, z component of angular momentum or parabolic quantum number (and any combination of these). Except for Refs. [6–8], these studies have been restricted to energies and fields such that the parabolic channels for a given core level are either all open or all closed.

The results presented in Refs. [8–13] did not contain energy regions near short range perturbers where the channel couplings, quantum defects, and oscillator strengths of the Rydberg states vary rapidly with energy due to their interaction with the perturber level; calculations are very difficult near perturbers (even in zero field) because the energy of the perturber and its interaction strength with the Rydberg series must be very accurate. In this paper, we specifically focus on the case near a short-range perturber where some of the parabolic channels are open and some are closed. The initial state is chosen so the perturber is strongly excited and governs the gross energy features of the photoionization cross section. This system was explored in Ref. [6] but with lower resolu-

tion and higher field strength; the rapid field induced ionization in that experiment allowed a simplified model calculation to qualitatively reproduce the data. We discuss why this model gave qualitative agreement.

II. MULTICHANNEL STARK THEORY

There have been many formulations of the behavior of Rydberg states in static electric fields. Because the Hamiltonian of a hydrogen atom in a static field separates in parabolic coordinates, the behavior of Rydberg states of nonhydrogenic systems may be described within a multichannel formalism. In this formalism, even a simple alkali-metal atom like Li has a multichannel behavior because the multiple channels are the channels in parabolic coordinates and the coupling between channels is provided by the nonhydrogenic potential generated by the core electrons; the coupling between the parabolic channels cannot change the electron's angular momentum in the direction of the electric field (assumed to be the *z*-direction in this paper). For more complicated atoms like Ar or Ba, the multichannel Rydberg interactions becomes even richer because the core electrons can scatter the Rydberg electron from one parabolic channel to another keeping all other quantum numbers fixed (this is similar to the Rydberg states of alkali-metal atoms) *and* can exchange energy and angular momentum in the *z* direction with the Rydberg electron; these scatterings or couplings cannot change the total angular momentum in the *z* direction.

We have based our treatment of Ba in a static field on the multichannel Stark theory developed in Ref. [5]. This formalism uses a local frame transformation between Coulomb functions in spherical and in parabolic coordinates to obtain the wave function and dipole matrix elements for nonhydrogenic atoms in static electric fields; it also uses an improved WKB method to quickly obtain the parameters in parabolic coordinates. The formalism developed in this section is very similar in spirit to the treatment presented in Refs. [12,13]. Although the method formulated in this section appears to be quite different from that in Refs. [12,13], the only real change is that we have removed the restrictions that all of the parabolic channels attached to a threshold be closed and that tunneling is negligibly slow. Our formulation also allows the calculation of the partial excitation amplitudes into all of the parabolic channels.

In H, the channels are labeled by ℓ,m in zero field and by β,m in a static electric field. Just as ℓ counts the number of nodes in the θ direction, the parameter β counts the number of nodes in the up-potential parabolic direction. The number of nodes in the up potential direction is often also denoted by n_1. Strictly speaking there are always an infinite number of nodes in the down potential parabolic direction. However, when the energy in the down potential direction is such that the electron has to tunnel to leave the region near the nucleus, then the number of nodes in the down potential direction for distances less than the maximum in the potential has a useful significance. We denote this number by the parameter n_2. When the energy width of a resonance is small compared to the spacing of resonances with the same n_1, then one can think of the resonance as having a principle quantum number given by $n=n_1+n_2+|m|+1$. Often, Stark resonances are labeled by n_1,n_2,m but another much used notation is n,k,m, where $k=n_1-n_2$. We will use both notations in this paper.

To prevent a lengthy rederivation of parameters, we present the ideas in this section as a continuation and amplification of the method described in Sec. IV of Ref. [14]. The derivation of our result will be presented for the alkali-metal atom case with the extension to atoms with multichannel states in zero-field given at the end of the section. As noted in Ref. [14] the dipole matrix elements connecting an initial state to a final state that has normalized outgoing waves in channel β is given by

$$d_\beta^- = (O^{-1}D^-)_\beta, \tag{1}$$

where O is the ''overlap'' matrix of parabolic continuum functions given by Eqs. (6) and (24) of Ref. [14] and the complex dipole matrix elements are defined by $D_\beta^- = \langle \Psi_{E\beta m}^- | \hat{\epsilon}\cdot\vec{r} | \Psi_I \rangle$, where Ψ_I is the initial state. The normalized continuum functions are given by Eqs. (20)–(22) of Ref. [14]. While this expression may be used to obtain the cross section and the partial cross sections into the different β channels, it is numerically inefficient to solve compared to expressions for cross sections given in Refs. [5,12,13]. The reason for the ineffeciency is that the O matrix has a size equal to the square of the number of parabolic channels. The expressions for the cross section in Refs. [5,12,13] involves matrix inversions where the matrices have a size equal to the square of the number of channels for which the zero-field quantum defects are not zero. However, Refs. [5,12,13] do not give expressions for amplitudes to escape in the different parabolic channels.

The dipole matrix elements in Eq. (1) may be expressed in terms of the zero-field dipole matrix elements using the zero-field wave functions with K-matrix normalization, D, and the zero-field phase shifts $K^0 \equiv \tan \pi\mu$ as

$$d^- = 2A^T[AA^\dagger + A^*A^T]^{-1}U^0D^0, \tag{2}$$

where $A=\bar{R}-U^0K^0(U^0)^T\bar{S}$ and $\bar{R},\bar{S}$ are given by Eq. (19) of Ref. [14] and U^0 is in Eqs. (15) and (16) of Ref. [14]. The superscript T indicates transpose of the matrix, the superscript * indicates complex conjugation of every element of the matrix, and the superscript † indicates Hermitian conjugation of the matrix. We note that the matrix A may be written as

$$A = U^0(1-K^0\Upsilon)(U^0)^{-1}\bar{R}, \tag{3}$$

with

$$\Upsilon = h^F - iH^F, \tag{4}$$

where the H^F and h^f matrices are defined in Eqs. (23) and (55) of the second part of Ref. [5]. After several matrix manipulations, the dipole matrix elements may be written as

$$d^- = 2(\bar{R}^*)^{-1}U^0d^F, \tag{5}$$

where

$$d^F = [H^F(1-K^0\Upsilon)^{-1}(1-K^0\Upsilon^*)+(1-\Upsilon^*K^0) \times (1-\Upsilon K^0)^{-1}H^F]^{-1}H^F(1-K^0\Upsilon)^{-1}D^0. \tag{6}$$

The reason for using Eqs. (5) and (6) instead of Eq. (1) is that all of the inverses in Eq. (6) are of matrices whose size equals the square of the number of channels with nonzero quantum defects; d^F is a complex vector whose size equals the number of channels with nonzero quantum defects. The matrix inverted in Eq. (5) is diagonal. Thus, these equations recover the efficiency of the method used in Ref. [5] while allowing the calculation of partial cross sections. The total cross section is given by

$$\sigma \propto \sum_{\ell,\ell'} (d^F_\ell)^* H^F_{\ell,\ell'} d^F_{\ell'}. \tag{7}$$

This method may be extended to systems that are multichannel in zero field by an appropriate extension of the definition of the matrices in Eqs. (5)–(7). We will let the parameter α indicate all of the zero-field channels that have nonzero K-matrix elements (i.e., these are the channels for which the Rydberg electron experiences non-Coulombic potential) [15]. In general, α describes five quantum numbers,

$$\alpha = \{N, J_i, M_i, \ell, m\}, \tag{8}$$

where J_i, M_i are the total and z component of all angular momenta except for the Rydberg electron, ℓ, m are the orbital angular momentum and the z component of the orbital angular momentum for the Rydberg electron, and N is all other quantum numbers. Note there is no coupling between states for which $M_i + m = M_{\rm tot}$ changes. To illustrate, we give three examples of α that are used in the Ba calculation. The three lowest energy states of Ba^+ are the $6s_{1/2}$, $5d_{3/2}$, and $5d_{5/2}$. Example 1: N is for the core electron to be in the $6s$ state with the spin of the Rydberg electron coupled to the core angular momentum to give angular momentum 0, $J_i = 0$, $M_i = 0$, $\ell = 2$, and $m = M_{\rm tot}$. Example 2: N is for the core electron to be in the $6s$ state with the spin of the Rydberg electron coupled to the core angular momentum to give angular momentum 1, $J_i = 1$, $M_i = -1$, $\ell = 3$, and $m = 1 + M_{\rm tot}$. Example 3: N is for the core electron to be in the $5d_{5/2}$ state with the spin of the Rydberg electron coupled to the core angular momentum to give angular momentum 3, $J_i = 3$, $M_i = 2$, $\ell = 4$, and $m = M_{\rm tot} - 2$.

In multichannel situations, Eqs. (5) and (6) are still correct when the matrices are generalized. In what follows, we will explicitly include the energy dependences with E being the total energy and E_N being the threshold energy with the ion having quantum numbers N. To simplify the formulas below, we define the parameter $\aleph$ to be the quantum numbers in parabolic coordinates,

$$\aleph = \{N, J_i, M_i, \beta, m\}, \tag{9}$$

which are similar to the α quantum numbers but with the angular momentum of the Rydberg electron replaced with the quantum number in the electric field, β. The extended matrices are given in an index notation as

$$H^F_{\alpha',\alpha} = \delta_{N',N}\delta_{J'_i,J_i}\delta_{M'_i,M_i}\delta_{m',m} H^F_{\ell',\ell}(E - E_N, m), \tag{10}$$

$$\Upsilon_{\alpha',\alpha} = \delta_{N',N}\delta_{J'_i,J_i}\delta_{M'_i,M_i}\delta_{m',m} \Upsilon_{\ell',\ell}(E - E_N, m), \tag{11}$$

$$U^0_{\aleph',\alpha} = \delta_{N',N}\delta_{J'_i,J_i}\delta_{M'_i,M_i}\delta_{m',m} U^0_{\beta',\ell}(E - E_N, m), \tag{12}$$

$$\overline{R}_{\aleph',\aleph} = \delta_{\aleph',\aleph}\overline{R}_\beta(E - E_N, m), \tag{13}$$

$$P^{N''}_{\alpha',\alpha} = \delta_{\alpha',\alpha}\delta_{N'',N'}\delta_{N'',N}, \tag{14}$$

where the last matrix, P, is a projection operator. The generalization of Eq. (7) is

$$\sigma \propto \sum_{\alpha,\alpha'} (d^F_\alpha)^* H^F_{\alpha,\alpha'} d^F_{\alpha'} \tag{15}$$

and the partial photoionization cross section to leave the ion with quantum numbers N is

$$\sigma(N) \propto \sum_{\alpha,\alpha',\alpha''} (d^F_\alpha)^* H^F_{\alpha,\alpha'} P^N_{\alpha',\alpha''} d^F_{\alpha''}. \tag{16}$$

These formulas reduce to those in Refs. [12,13] when the energy of the outer electron is either positive ($E - E_N > 0$) or much less than the energy needed for a classical electron to escape the ion ($E - E_N \ll -2\sqrt{F}$) in all of the channels. In the situations we investigated, the energy of the outer electron in some of the channels is negative but greater than the energy needed for a classical electron to escape (i.e., $-2\sqrt{F} < E - E_n < 0$); thus, the full treatment is needed. The amount of computational effort necessary to obtain the total and partial cross sections is quite modest, with the most time-consuming steps being the inversion of two complex matrices, $1 - K^0\Upsilon$ and the term in square brackets of Eq. (6), at every energy point; the size of both of these matrices is the square of the number of α channels. However, the spectra for the cases we investigated consist of a very large number of sharp resonances so we need to calculate the cross section at a large number of points; the effeciency gained in going from Eq. (1) to Eq. (5) makes the calculation possible.

We have stated that Eq. (5) was necessary because some of the parabolic channels attached to the $6s$ threshold are open and some are closed; the closed parabolic channels give the resonances associated with Rydberg states in an electric field. The ''quasidiscrete'' approximation used in Refs. [12,13] would give poor results for our case. In a typical calculation (e.g., for a field of 1.6 kV/cm), there are 20 open and 62 closed parabolic channels 20 $\rm cm^{-1}$ below the $5d7d\,{}^1D_2$ perturber but 48 open and 38 closed 20 $\rm cm^{-1}$ above the perturber.

The WKB method we used is quite accurate for the channels attached to the $6s$ threshold but could *not* be used for the channels attached to the $5d$ thresholds. Small inaccuracies from WKB phases and couplings give relatively large energy errors in the $5d$ channels. In general for a phase error δ, the energy error is $\sim \delta/(\pi\nu^3)$ in a.u. where $\nu \sim 25$ in the $6s$ channel but $\nu \sim 4.65$ in the $5d$ channels. The $5d7d\,{}^1D_2$ perturber is shifted by ~ 20 $\rm cm^{-1}$ from its correct position when using the WKB approximation for the $5dn\ell$ channels. Thus it is a much better approximation to ignore the effect of the electric field in the $5d$ channels and use the zero-field

TABLE I. Zero-field experimental [1] and calculated $J=2^e$ energy levels in cm^{-1}. The calculated oscillator strength f in arbitrary units and the squared mixing coefficients of the $6snd\,^1D_2$, $6snd\,^3D_2$, and perturber are presented. The experimental energies have been rounded to the nearest 0.1 cm^{-1}.

Desig.	$E_{expt.}$	$E_{calc.}$	f	$^1D_2$	$^3D_2$	Pert.
$6s24d\,^3D_2$	41 790.8	41 790.6	0.9	0.15	0.84	0.01
$6s24d\,^1D_2$	41 792.6	41 792.7	1.1	0.83	0.16	0.01
$6s25d\,^3D_2$	41 811.9	41 811.8	2.6	0.27	0.70	0.03
$6s25d\,^1D_2$	41 813.6	41 813.7	1.6	0.69	0.29	0.01
$6s26d\,^3D_2$	41 829.5	41 829.4	11.4	0.47	0.39	0.11
$6s26d\,^1D_2$	41 831.9	41 832.0	1.9	0.39	0.59	0.02
$5d7d\,^1D_2$	41 841.7	41 841.7	34.3	0.47	0.13	0.39
$6s27d\,^3D_2$	41 848.3	41 848.2	1.3	0.12	0.87	0.01
$6s27d\,^1D_2$	41 852.1	41 852.0	16.6	0.73	0.07	0.19
$6s28d\,^3D_2$	41 862.7	41 862.6	0.7	0.03	0.97	0.01
$6s28d\,^1D_2$	41 864.7	41 864.7	4.0	0.93	0.02	0.05

quantum-defect formulas to close these channels. This is an excellent approximation due to the compact nature of the perturber.

III. ZERO-FIELD THEORY OF BA

The zero-field K matrices and dipole matrix elements in jQ coupling [16] are the main input into the calculations; in this coupling scheme the total angular momentum of the core electron is first coupled to the spin of the Rydberg electron to give an angular momentum Q and then the orbital angular momentum of the Rydberg electron is coupled to Q to give the total angular momentum J. This is the most convenient coupling scheme since the electric field acts on the ℓ of the outer electron and matches the coupling scheme given by the α quantum number in Eq. (8).

The K matrices and dipole matrix elements are obtained in LS coupling using R-matrix codes and then transformed into jQ coupling using a frame transformation. These should be very good approximations, but for our system this procedure did not work well enough because small errors in the quantum defect produce relatively large errors in the perturber position; e.g., our first calculation gave a perturber energy 15 cm^{-1} too low (an error of 0.007 in the quantum defect). It was necessary to apply small corrections to the LS-coupled K matrices in order for all of the perturber and Rydberg states to be at their proper *zero-field* positions. Small errors in the $6sn\ell$ quantum defects had little effect on our Stark calculations; however, we did correct them to be consistent in our treatment of the $6s$ and $5d$ channels. Maximum changes in quantum defects and mixing angles were less than 0.01. In Table I, we give the calculated (from corrected K matrices) and experimental zero-field energy levels for the $J=2^e$ levels near the perturber with our calculated oscillator strengths and squared mixing coefficients. Most of the spin-orbit effects arise through the spin-orbit splitting of the $5d$ thresholds whose energies were obtained from experiment; the direct spin-orbit interaction for the Rydberg electron has little effect on the dynamics.

The sequence of recouplings, which we needed to perform to obtain the parameters in the α coupling scheme, involve standard atomic parameters. The transformation of the dipole matrix elements and K matrices from LS coupling to jQ-coupling uses the unitary matrix

$$\langle LS|jQ\rangle^J=\langle (L_c\ell)L(S_cs)S|[(L_cS_c)j_cs]Q\ell\rangle^J, \quad (17)$$

where L_c, S_c are the total orbital angular momentum and spin of the core, ℓ, s are the orbital angular momentum and spin of the Rydberg electron, j_c is the total angular momentum of the core, Q is the angular momentum obtained by coupling the angular momentum of the core to the spin of the Rydberg electron, and J is the total angular momentum. This unitary matrix is the product of two $6j$ coefficients and simple factors that depend on the angular momenta,

$$\langle LS|jQ\rangle^J=-1^{L+S+\ell+2Q+L_c+S_c+s}[L,Q,S,j_c] \times\begin{Bmatrix}\ell & L_c & L\\ S & J & Q\end{Bmatrix}\begin{Bmatrix}L_c & S_c & j_c\\ s & Q & S\end{Bmatrix}, \quad (18)$$

where $[j]=\sqrt{2j+1}$.

This recoupling is not sufficient to obtain quantum numbers in the form α of Eq. (8). We need to isolate the angular momentum of the Rydberg electron and its z component. This is accomplished through one last recoupling that uncouples the Q and ℓ angular momenta. This is accomplished through another unitary matrix that is simply a Clebsch-Gordon coefficient,

$$\langle JM|m_Q,m\rangle=\langle Qm_Q\ell m|Q\ell JM\rangle, \quad (19)$$

where Q, m_Q are the J_i, M_i of the α quantum number. After this sequence of recouplings, the K matrices and dipole matrix elements are in the form used in the preceding section.

The initial state is the $5d6p\,^3D_1^o$ excited state 24 192.1 cm^{-1} above the ground state [17] (all energies are rounded to the nearest 0.1 cm^{-1}, since this is the resolution of our laser system). In the calculation, this state was obtained by diagonalization of a large basis of two electron states, all of which had $^3D^o$ character. Thus the electrostatic part of the correlation is reproduced very accurately. However, we have completely neglected the correlation due to relativistic effects, which can mix these states with other states of the same total angular momentum and parity but different LS. This is a good approximation since the amount of mixing of this state with states of $^3P^o$ or $^1P^o$ character is small. Since oscillator strength from the $^3D^o$ state to the $5d7d\,^1D_2$ perturber is quite large, the neglect of the small mixing of the initial states with other states of different LS but the same total angular momentum and parity has very little effect on the calculation.

Before examining the couplings in a static field, it is important to first understand the zero-field behavior. There are two perturbers in the energy range we examined, and due to our excitation scheme only one of them has a substantial effect on the atomic correlation in a static electric field. We concentrate on the zero-field behavior of this perturber, $5d7d\,^1D_2$, because it is the energy dependence of the dipole matrix elements, quantum defects, and singlet-triplet mixing that distinguishes this system from the alkalilike systems previously investigated. The square of the mixing coefficients in Table I shows that to a large extent the perturber

controls the mixing between the ^1D and ^3D channels. For example, the 26d states are almost equal admixtures of singlet and triplet character, whereas the 28d states are nearly pure, and the oscillator strength is nearly proportional to the perturber fraction. Because the initial state is $^3D^o$, this shows that the perturber has a large fraction of triplet character even though it is designated ^1D. In fact, the perturber is roughly an equal admixture of $^1D_2$ and $^3P_2$, $^3D_2$, $^3F_2$ character. Dynamics near the perturber is governed by the interactions

$$6snd\,^1D_2 \leftrightarrow 5d7d\,^1D_2 \leftrightarrow 6snd^3D_2. \tag{20}$$

The double arrows in this equation are meant to indicate the effect on the dynamics from electron correlation. Note, there is no direct interaction between the $6snd\,^1D_2$ and $^3D_2$ states within our calculation so this interaction must be mediated by the perturber.

We stress that while the small changes made to the LS-coupled K matrices caused the agreement between the experimental and calculated energies to be quite good this does not guarantee that the correlations will be correctly reproduced. In particular, the method we used to include relativistic effects (the LS-to-jQ frame transformation) is an approximation that neglects some of the relativistic interactions. The main interaction that is missing causes nonzero terms in the K matrix that connect channels with different LS but the same J. For the alkaline earth atoms, these terms are small except for Ra; therefore, only parameters that depend on sensitive standing wave behavior in the Ba Rydberg series will be strongly affected. Another way of stating this is that small couplings can only have a large effect if there is a near degeneracy of energy levels. As discussed below, the electric fields we used in our investigation caused the Rydberg states to autoionize thus the correlation from weak interactions does not have a chance to occur.

A much larger source of error in the calculation arises because the K matrices were only corrected to obtain the experimental zero-field energies. By only trying to improve the agreement with the experimental energies, we did nothing to directly improve the singlet-triplet mixing between states or the dipole matrix elements between the initial and final states. However, we found that the results from the R-matrix calculations were accurate enough to explain the gross features in the experiment. Simultaneous fitting of energy levels, mixing coefficeints, and dipole matrix elements would be a very big job without a large increase in the accuracy of the calculations.

A final aspect of the zero-field final-state correlation is the positions of other short-range perturbers that could affect the calculation. The state closest to the $^1D_2$ perturber is the $5d7d\,^3F_4$ perturber [3] which is only 4 cm^{-1} above the $^1D_2$ perturber. No other short-range perturbers are within the energy range we investigated. The next two closest states are the $5d7d\,^3F_3$ perturber [3], which is 115 cm^{-1} below and the $5d7d\,^3P_1$ perturber [1], which is 89 cm^{-1} above the $^1D_2$ perturber.

IV. EXPERIMENTAL PROCEDURE

A schematic drawing of the experimental arrangement is given in Fig. 1. In the experiment, we crossed two narrow bandwidth lasers in a vacuum chamber with an atomic Ba beam and measured the electron yield versus wavelength. The two ns dye lasers were both pumped with the frequency doubled output of a ns neodymium-doped yttrium aluminum garnet (Nd:YAG) laser at 532 nm. The output of the first dye laser (676 nm) was mixed with the fundamental of the Nd:YAG laser (yielding 413.4 nm) and used to excite the Ba atoms from the $6s^2$ to the $5d6p\,^3D_1$ state; the polarization of this laser was always chosen to be parallel to the static electric field so the initial state was always $M=0$. The frequency of the second dye laser was scanned over an energy range covering the $5d7d\,^1D_2$ perturber (around 566 nm). This laser's intensity was kept low (~ 5 MW) to prevent saturation of the resonances and was polarized either parallel or perpendicular to the static electric field; thus the final state could be chosen to be $M=0$ or $M=1$. The scanning laser has a resolution of 0.1 cm^{-1}, which is sufficient to resolve many of the lines and distinguish most of the Stark resonances that have strength 20% above the background. In order to be able to calibrate this laser a lamdascope [18] was used. In this way we achieved an error in the calibration of 0.1 cm^{-1}.

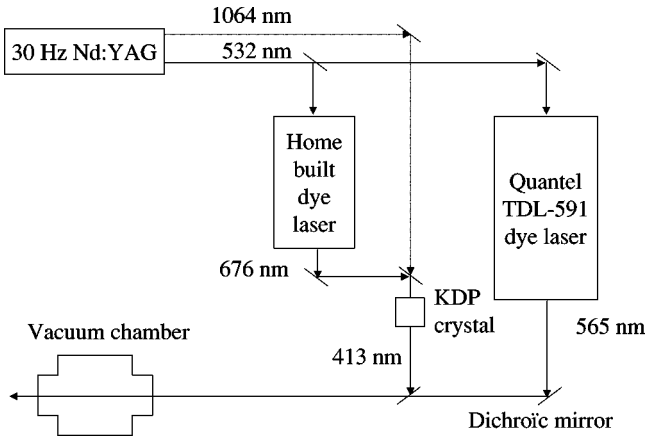

FIG. 1. Setup for the absorption spectroscopy experiment. A Nd:YAG laser is used to pump two pulsed ns dye lasers, operating at 30 Hz. The output of the first ns dye laser is used to produce photons of 413.4 nm by mixing it with the fundamental of the Nd:YAG laser (1064 nm). The output of the second ns dye laser is delayed by approximately 50 ns with respect to the 413.4-nm photons and aligned collinear with the 413.4-nm beam into the vacuum chamber. The colinear beams interact in a crossed-beam arrangement with a thermal barium beam in between two capacitor plates. A set of multichannel plates is used to record the ionized electrons.

The static electric field was realized by two parallel capacitor (diameter: 5.0 cm) plates 10.0 mm apart in a cylindrical symmetric orientation. In between the capacitor plates a thermal barium beam was created by a resistively heated oven in which solid barium was placed. This oven has a 1 mm diameter hole through which gas-phase barium atoms could escape and thus form a beam. The direction of the lasers was aligned perpendicular to the barium beam in between the plates. In order to be able to detect the ionized electrons a hole (with a diameter of 7.0 mm) was drilled through the center of the plate with the highest potential, so that these electrons could travel out of the interaction regions towards a set of multichannel plates. The electron yield on the detector is recorded as a function of the wavelength of the second laser.

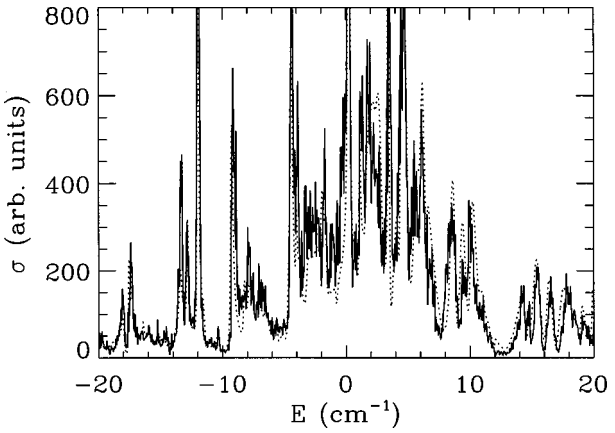

FIG. 2. Photoionization cross section of Ba from the $5d6p\ ^3D_1$ $M=0$ initial state. The energy is relative to the zero-field position of the $5d7d\ ^1D_2$ perturber. The laser is polarized parallel to the electric field of 1600 V/cm. The solid line is the experiment and the dotted line is the calculation.

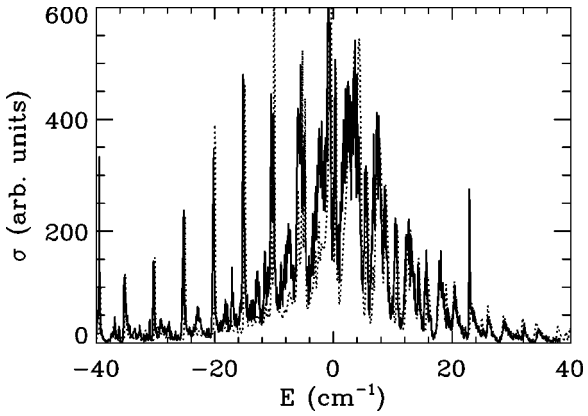

FIG. 3. Same as Fig. 2 except the laser is polarized perpendicular to the electric field of 1820 V/cm.

There are several possible sources of incorrect structure in the experimental cross section that contribute very little signal using our experimental setup. Two photon ionization from the $5d6p\ ^3D_1$ state did not contribute any noticeable signal to the experiment because the second laser was greatly reduced in intensity to prevent one photon saturation of the resonances. The second dye laser could not two-photon ionize Ba from the $6s^2$ state, which eliminated another possible source of erroneous resonance structure. The only possible ''wrong'' two-photon signal is from absorption by Ba of two photons from the first laser which can resonantly excite Ba atoms from the $6s^2$ to the $5d6p\ ^3D_1$ state and then into the continuum with the second photon. However, this process will only give a constant background, since the frequency of this laser was fixed. As can be seen in the figures, the background signal is weak.

V. RESULTS

The calculations were performed using several approximations and the excellent agreement between calculation and experiment validates these approximations. This gives some information about the dynamics. The main approximation involved separating the wave function so that the Rydberg electron near the core was described in spherical coordinates, while far from the core it was described in parabolic coordinates. The wave function in parabolic coordinates was determined using the WKB method of Ref. [5].

In Figs. 2 and 3, we present the experimental and calculated photoabsorption cross section of Ba atoms in an electric field versus energy relative to the $5d7d\ ^1D_2$ zero-field position: 41 841.7 cm^{-1} above the $6s^2$ ground state. The initial state is the $5d6p\ ^3D_1$ state with total angular momentum in the field direction $M=0$. Because the initial state is compact and the electric fields are weak, we always use a zero-field initial state in the calculation. One photon from this initial state strongly excites the perturber with very little direct excitation of the $6snl$ Rydberg states. The photoexcited Rydberg states are all located above the saddlepoint of the potential and are autoionizing states. In Fig. 2 the electric field strength is 1600 V/cm and the lasers are polarized so that only $M=0$ final states are populated. In Fig. 3 the electric field strength is 1820 V/cm and the lasers are polarized so that only $M=1$ final states are populated. We have performed comparisons between experiment and calculation for several different field strengths for each polarization; the comparisons were uniformly as good as those in Figs. 2 and 3. The agreement between experiment and theory is excellent over the full range explored: -50 cm^{-1} to 50 cm^{-1} although we only present a fraction of this range for clarity. The broad feature with an energy width ~ 15 cm^{-1} arises from the $5d7d\ ^1D_2$ perturber. The sharper features arise from resonances in the closed parabolic channels and are strongly perturbed blue Stark states, $6snk$, with principle quantum number $n\sim 20-26$.

We have not presented the data in a Stark map form because even at the lowest fields where data can be acquired the levels are in the n-mixing regime. There are three obvious trends in the spectra as the field strength increases. The first trend is that the broad envelope of excitation does not change with field strength because the envelope arises from the $5d7d$ perturber, which is not affected by the fields used in our experimental arrangement (fields were less than 3 kV/cm). The second trend is that the number of visible Stark resonances decreased with increasing field strength; this is because the number of levels within the $n=21-26$ manifolds that are below the saddle point in the potential decreases with increasing field strength. The third trend is the energy widths of the Stark resonances increase with increasing field strength; this is because at a fixed energy the anglular range where the electron can leave the Ba^+ core and classically escape increase with increasing field strength.

The positions of the Stark states of H do not match the positions of the resonances very well because the perturber causes substantial intensity modulations and energy shifts of the Stark states. The classification of the resonances thus has relatively little meaning. However, to obtain some idea of what states participate in the figures we give the energies and classifications of the lowest and highest energy state of each n manifold in Tables II and III that would appear in Figs. 2 and 3. The principle quantum number is given by $n=n_1+n_2+|m|+1$, where n_1 is the number of nodes in the up potential parabolic wave function and n_2 is the number of nodes in the down potential parabolic wave function. For example in Fig. 2, there are two $n=21$ states, (19,1) and

TABLE II. Energies and classification of the lowest energy resonance for each H Stark n manifold shown in Fig. 2. $m=0$ and $F=1600$ V/cm. n_1 is the number of nodes in the up potential direction.

n_1	n_2	n	$E(\mathrm{cm}^{-1})$
19	1	21	−18.3
20	0	21	−13.9
15	6	22	−15.5
21	0	22	12.1
11	11	23	−17.5
18	4	23	16.0
8	15	24	−19.2
15	8	24	15.9
6	18	25	−19.7
13	11	25	17.0
5	20	26	−18.9
11	14	26	14.7

(20,0), and there are 7 $n=22$ states, (15,6), (16,5), (17,4), (18,3), (19,2), (20,1), and (21,0). In a given n manifold, the energies of the states increase monotonically with the number of nodes in the up potential parabolic wave function. Using Table II, one can compute that 40 resonances for H are in the energy range in Fig. 2; the number for Ba is roughly four times as many.

In Fig. 4 we present the results of a calculation of the partial singlet and partial triplet photoionization cross sections which clearly demonstrate the change in the correlation due to the electric field. The partial singlet photoionization cross section is the cross section for photoionization with the electron spins coupled to total spin 0 [19]. The sum of these two cross sections equals the total cross section in Fig. 3. Some aspects of the partial cross section are understandable from the data in Table I. For example, the zero-field states more than 7 cm^{-1} above the perturber do not have a strong singlet-triplet mixing and the singlet oscillator strengths are much larger than for triplet states. This implies that the singlet partial cross section should be much larger than the triplet for energies larger than 7 cm^{-1} which agrees with Fig. 4. But some aspects of the partial cross section could not be

TABLE III. Same as Table II but for $m=1$ and $F=1820$ V/cm shown in Fig. 3.

n_1	n_2	n	$E(\mathrm{cm}^{-1})$
14	5	21	−35.8
19	0	21	−10.9
10	10	22	−36.8
20	0	22	15.5
7	14	23	−37.6
21	0	23	39.1
5	17	24	−37.4
18	4	24	37.2
4	19	25	−35.7
16	7	25	37.1
11	13	26	13.4
15	9	26	39.5

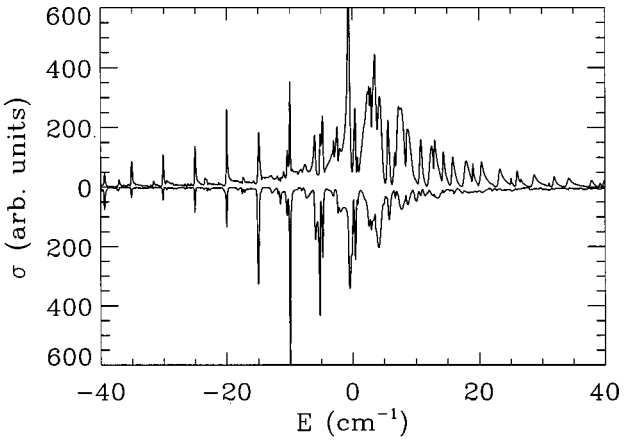

FIG. 4. Upper curve is the calculated singlet partial photoionization cross section and the reflected curve is the calculated triplet partial photoionization cross section. The laser is polarized perpendicular to the electric field of 1820 V/cm. Except for the sharpest resonances between −16 and 0 cm^{-1} the singlet cross section is much larger than the triplet cross section, which seemingly contradicts the information on the 24-26d states in Table I.

predicted from the information in Table I. For example, there are few energies where the triplet partial cross section is larger than the singlet cross section. Only at the sharp resonances at −15, −10, and −5 cm^{-1} is the triplet cross section larger than the singlet. This is contrary to what might be expected from the zero-field data of Table I but may be explained by the qualitative change in dynamics in the electric field.

VI. DISCUSSION

We have performed a number of calculations to determine how the correlation is modified by the strong electric field. In one test, we performed a calculation where we closed the $5d$ channels correctly but after closing these channels we set the coupling between the $6sn\ell$ singlet and triplet channels to zero. The agreement between this calculation and the correct calculation was surprisingly good because the channel mixing between $6snd$ singlet and triplet channels in Table I is strongly reduced in an electric field. This result affects the interpretation of Ba dynamics near the $5d7d\,^1D_2$ perturber. The mixing coefficients and oscillator strengths in Table I result from a delicate balance of standing wave behavior represented by the double-headed arrows in Eq. (20). In the electric field, the $5d7d\,^1D_2$ perturber decays into singlet and triplet Stark channels with some channels open and some closed. If the electron is ejected into an open channel, it leaves the atom. If the electron is ejected into a closed channel, a resonant Stark state can be excited. However, because the Stark states can decay to a continuum, there is relatively little chance for the electron to be captured from the Stark state into the perturber and be converted from singlet to triplet or vice versa. The correlation in an electric field may be represented by

$$6snk\,^1K \leftarrow 5d7d\,^1D_2 \rightarrow 6snk\,^3K, \qquad (21)$$

where k is meant to represent a Stark state. Only the sharpest resonances have a long enough lifetime to acquire substantial singlet-triplet mixing. This explains the lack of coupling demonstrated in our test calculation. It also explains why the $5d7d\,^3F_4$ state which is 4.0 cm^{-1} above the $^1D_2$ has *no* visible effect on the cross section.

The reason that mainly singlet states are excited (see Fig. 4) may again be related to the dynamics of Eq. (21). We should not use the oscillator strengths in Table I to estimate what will happen in a strong static field. If we want to compare to zero-field data we should ask how would the $5d7d\,^1D_2$ state evolve if the $6s$ threshold were lowered so this perturber becomes an autoionizing state. We have performed this zero-field photoionization calculation with the $6s$ threshold artificially lowered so that the $5d7d\,^1D_2$ state was an autoionizing state and one of the electrons can escape. At -30 cm^{-1} the singlet partial cross section was 5.7 times larger than the triplet partial cross section, at 0 cm^{-1} it was 4.2 times larger, and at 30 cm^{-1} it was 2.8 times larger. This agrees with the results presented in Fig. 4.

It may be somewhat surprising that exciting a resonance state that has mostly triplet character from an initial state that has purely triplet character can produce ejection mainly into singlet continua. This is a manifestation of the electron correlation and propensity rules. Without the spin orbit interaction, the $^3P_2$ states and $^3F_2$ states cannot interact with $6s\varepsilon\ell$ continua and decay. It is only the $^3D_2$ and $^1D_2$ states that can autoionize without the spin orbit interaction. In the zero-field probability to scatter from the $5dnd$ channel to the $6s\varepsilon\ell$ continua, the ^1D channel scattered roughly 4 times more strongly than the ^3D channel. The stronger ^1D coupling to the continuum arises because the triplet wave function has a node when the electrons are at the same position which suppresses the electron-electron interaction for the triplet states. This implies that the $5d7d\,^1D_2$ perturber decays preferentially into the ^1D continuum because the ^1D part of the perturber decays most easily.

The fact that mainly singlet Stark series are excited explains one of the mysteries of the spectra: only a small fraction ($\sim 25\%$) of the Stark resonances are visible. For every singlet Stark state there are three triplet Stark states that have relatively little oscillator strength. In fact, we were able to get rough agreement with the full calculation by performing an alkali-atom type of calculation with ℓ quantum defects equal to the Ba ^1L quantum defects for $\ell \neq 2$ and for $\ell = 2$ using a quantum defect that increased by 1 over an energy range comparable to the width of the perturber. This also explains why Ref. [6] could obtain qualitative agreement between their experimental results at high fields and their one-channel model.

In conclusion, we have experimentally measured and calculated the photoionization cross section of Ba in a strong electric field. The dynamics near the $5d7d\,^1D_2$ perturber was surprisingly simple and could be explained by the change in the multichannel dynamics in the static field. This study emphasizes the fact that configuration interaction depends on both the short-range interactions between channels and the long-range dynamics of the Rydberg electron; the resonances must exist long enough for configuration interaction to fully develop. Surprisingly, static fields can sometimes suppress complications existing in zero-field processes.

The formalism developed in this paper opens a new avenue of investigation of atoms in electric fields since we give formulas for the asymptotic form of the multichannel wave function. Several interesting questions may now be addressed. For example, we can now investigate the dynamics of Ba in a static electric field as probed by measuring the time dependence of the electrons ejected from the atom. We can also investigate the role that scattering in a static field plays on branching ratios for decay into different open channels. The spatial distribution of the electrons ejected from an atom can be calculated. The role of semiclassical and classical catastrophes (like bifurcations) in the scattering between open and closed channels can also be investigated. These and other questions will be addressed in the near future.

ACKNOWLEDGMENTS

F.R. was supported by the NSF. C.W. and L.D.N. were supported by the Stichting Fundamenteel Onderzoek van de Materie (FOM) and also financially supported by the Nederlandse Organisatie voor Wetenschappelijk Onderzoek (NWO). Computations were performed at the National Energy Research Supercomputer Center in Berkeley, CA.

[1] M. Aymar, P. Camus, M. Dieulin, and C. Morillon, Phys. Rev. A **18**, 2173 (1978); M. Aymar and O. Robaux, J. Phys. B **12**, 531 (1979).

[2] M. Aymar, C. H. Greene, and E. Luc-Koenig, Rev. Mod. Phys. **68**, 1015 (1996).

[3] P. Camus, M. Dieulin, and A. El Himdy, Phys. Rev. A **26**, 379 (1982).

[4] W. Vassen, E. Bente, and W. Hogervorst, J. Phys. B **20**, 2383 (1987).

[5] D. A. Harmin, Phys. Rev. A **24**, 2491 (1981); **26**, 2656 (1982).

[6] W. Sandner, K. A. Safinya, and T. F. Gallagher, Phys. Rev. A **33**, 1008 (1986).

[7] C. Blondel, R.-J. Champeau, and C. Delsart, Phys. Rev. A **27**, 583 (1983).

[8] A. König, J. Neukammer, H. Hieronymous, and H. Rinneberg, Phys. Rev. A **43**, 2402 (1991).

[9] C. Delsart and J.-C. Keller, Phys. Rev. A **28**, 845 (1983).

[10] W. E. Ernst, T. P. Softley, and R. N. Zare, Phys. Rev. A **37**, 4172 (1988).

[11] T. P. Softley, A. J. Hudson, and R. Watson, J. Chem. Phys. **106**, 1041 (1997).

[12] D. J. Armstrong, C. H. Greene, R. P. Wood, and J. Cooper, Phys. Rev. Lett. **70**, 2379 (1994).

[13] D. J. Armstrong and C. H. Greene, Phys. Rev. A **50**, 4956 (1994).

[14] F. Robicheaux and J. Shaw, Phys. Rev. A **56**, 278 (1997).

[15] We note that all channels have K-matrix elements that are nonzero. However, the size of the K-matrix elements decreases

very rapidly with the orbital angular momentum of the Rydberg electron. For the level of accuracy desired in a particular problem, there is an effective maximum orbital angular momentum where *K*-matrix elements for higher angular momentum may be set identically to zero without affecting the calculation.

[16] F. Robicheaux and W. T. Hill III, Phys. Rev. A **54**, 3276 (1996).

[17] *Atomic Energy Levels*, edited by C. E. Moore, Natl. Bur. Stand. (U.S.) Circ. No. 467 (U.S. GPO, Washington, DC, 1949).

[18] N. Pelletier-Allard and R. Pelletier, Rev. Sci. Instrum. **55**, 1442 (1984).

[19] The singlet and triplet partial cross sections are well defined because once the electron leaves the atom there is no interaction that changes the spin coupling since the core is left in an *s* state.